Transition Met Chem (2014) 39:111–118
DOI 10.1007/s11243-013-9779-4

Crystal structures, cyclic voltammetry and DNA binding of two mononuclear nickel(II) complexes

Yang Wang · Jia-Wei Mao · Chao Ding · Zhi-Quan Pan · Jian-Fen Li · Hong Zhou

Received: 29 August 2013 / Accepted: 29 October 2013 / Published online: 12 November 2013

Abstract Two unsymmetrical complexes, $[NiL^1]ClO_4$ (**1**) and $[NiL^2]ClO_4$ (**2**) have been synthesized and characterized by IR, UV, ES-MS and single crystal X-ray diffraction, where HL^1 and HL^2 are, respectively, the [1+1] condensation products of 2,6-diformyl-4-X-phenol (X = F or CH_3) with N^1-(2-aminoethyl)-N^2-(4-nitrobenzyl) ethane-1,2-diamine. The coordination geometry of the metal in both complexes can be approximately described as square planar with a mean plane deviation of 0.032 Å in complex **1** and 0.027 Å in complex **2**, respectively. The binding activities of the complexes toward calf-thymus DNA have been analyzed by spectroscopy and viscosity methods. The binding constants of **1** and **2** obtained from UV spectroscopic studies are 5.43×10^5 and 1.83×10^5 M^{-1}, respectively, while the linear Stern–Volmer quenching constants obtained from fluorescence spectroscopic studies are 0.83×10^3 and 0.71×10^3 M^{-1}, respectively. The cyclic voltammograms of the complexes show a pseudo-reversible electrochemical process.

Electronic supplementary material The online version of this article (doi:10.1007/s11243-013-9779-4) contains supplementary material, which is available to authorized users.

Y. Wang · J.-F. Li
School of Chemical and Environmental Engineering, Wuhan Polytechnic University, Wuhan, People's Republic of China

Y. Wang · J.-W. Mao · C. Ding · Z.-Q. Pan · H. Zhou (✉)
Key Laboratory for Green Chemical Process of Ministry of Education, Wuhan Institute of Technology, Wuhan, People's Republic of China
e-mail: hzhouh@126.com

J.-W. Mao
National Quality Supervision and Inspection Center For Petroleum and Natural Gas Products, Sichuan Institute of Product Quality Supervision and Inspection, Chendu, People's Republic of China

Introduction

Schiff base complexes play a significant role in the field of coordination chemistry and have been extensively studied, mainly due to their structural varieties and structure-related bioactivities [1–4]. Schiff base complexes can be used as DNA structural probes, oxidation catalysts, DNA cleaving agents, potential anticancer drugs, enzyme models and so on [5–8]. In general, the bioactivities of such complexes depend on the structures of the ligands and the metal types. They can bind to DNA in many non-covalent modes, involving ionic bonding, hydrogen bonding and hydrophobic interactions, and many can cleave the DNA. Complexes with aromatic rings can bind DNA through π–π stacking as well as coordination interactions with the metal center. Our previous studies showed that dinuclear Ni(II) complexes containing three benzyl groups have interesting DNA cleavage and binding activities [9]. In continuation of this approach, two mononuclear Ni(II) complexes $[NiL]^+$, where HL is the [1+1] condensation product of the same aldehyde with different amines, have been synthesized and characterized. The DNA binding activities of these complexes have been also investigated. The synthesis of the complexes is shown in Scheme 1.

Experimental

All solvents were obtained from commercial sources and used without purification. The aldehydes 2,6-diformyl-4-X-phenol (X = F or CH_3) were prepared according to the

Scheme 1 The synthesis of the complexes

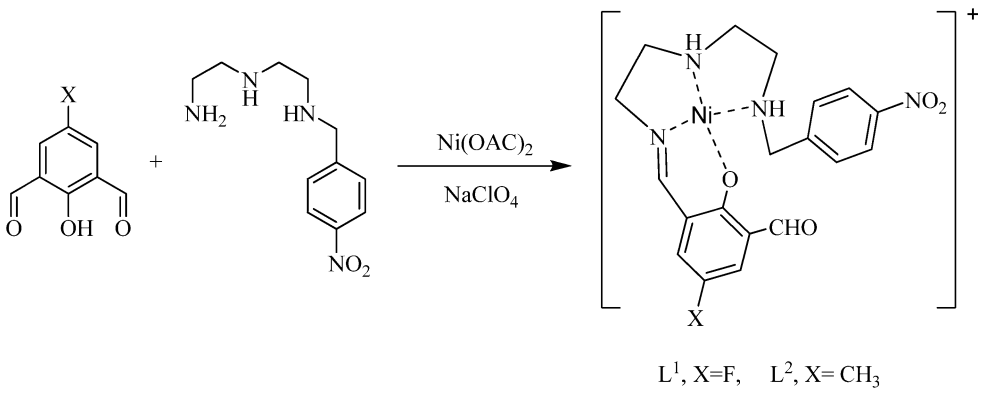

L^1, X=F, L^2, X= CH_3

literature methods [10, 11]. N^1-(2-aminoethyl)-N^2-(4-nitrobenzyl)ethane-1,2- diamine was prepared by our previous method [9]. Tris(hydroxymethyl)amino-methane (Tris) and ethidium bromide (EB) were purchased from Toyobo Co. Calf-thymus DNA(CT-DNA) was obtained from Sigma.

IR spectra were measured using KBr disks on a Vector 22 FT-IR spectrophotometer. Elemental analyses were performed on a Perkin–Elmer 240 analyzer. Electrospray mass spectra were determined on a Finnigan LCQ, using methanol as mobile phase, and a sample concentration of 1.0 mmol/dm^3. UV–Vis spectra were recorded on a UV-2450 spectrophotometer. Fluorescence spectroscopic studies were carried out on an F-7000 FL Spectrophotometer. Cyclic voltammograms were run on a CHI model 750 B electrochemical analyzer in DMF solution containing tetra(n-butyl)ammonium perchlorate (0.1 M) as the supporting electrolyte. A three-electrode cell was used, which was equipped with a glassy carbon-working electrode, a platinum wire as the counter electrode and a Ag/AgCl electrode as the reference electrode. Scanning rates were in the range of 50–200 mV s^{-1}. Half-wave potentials, $E_{1/2}$, were the average of E_{pa} and E_{pc}, the measured error was ±2 mV. Viscosity experiments were conducted on an Ubbelohde viscometer.

Preparation of $[NiL^1]ClO_4$ (1)

To a solution of 2,6-diformyl-4-fluorophenol (0.084 g, 0.5 mmol) and $Ni(OAc)_2{\cdot}4H_2O$ (0.124 g, 0.5 mmol) in anhydrous ethanol (15 mL), a mixture of N^1-(2-aminoethyl)-N^2-(4-nitrobenzyl)ethane-1,2-diamine hydrobromide (0.241 g, 0.5 mmol) and NaOH (0.060 g, 1.5 mmol) in distilled water (10 mL) was added dropwise. The mixture was stirred at ambient temperature for 8 h followed by addition of $NaClO_4$ (0.070 g, 0.5 mmol). The resulting solution was stirred for further 8 h and filtered. Orange block crystals suitable for the X-ray measurement were obtained by evaporation of the filtrate at room temperature for 2 weeks. Yield: 0.104 g (38 %). Anal. Calc. for $C_{19}H_{20}N_4FNiO_4ClO_4$ (%): C, 41.8; H, 3.7; N, 10.3. Found: C, 41.6; H, 3.4; N, 10.6. IR(KBr, ν/cm^{-1}): 3,209 ν(N–H), 1,635 ν(C=N), 1,688 ν(C=O), 1,094, 624 $\nu(ClO_4^-)$.

Table 1 Crystal data and structure refinement for complex **1**

Empirical formula	$C_{19}H_{20}FN_4NiO_4ClO_4$
Formula weight	545.55
Crystal system	Triclinic
Space group	P-1
a (Å)	9.3562(15)
b (Å)	9.7874(16)
c (Å)	13.700(2)
α (°)	110.688(2)
β (°)	96.185(2)
γ (°)	106.833(2)
Volume (Å^3)	1,092.0(3)
Z	2
D (calc) (g/cm^3)	1.659
Mu (Mokα) [/mm]	1.075
F(000)	560
Crystal size[mm]	0.22 × 0.24 × 0.28
Temp., K	293
Mo Kα radiation(Å)	0.71073
θ range (deg)	2.3, 26.0
Nref, Npar	4204, 307
Tot., uniq. data *R*(int)	6098, 4204, 0.003
Observed data [I > 2.0sigma(I)]	3473
R, wR$_2$, S	0.0549, 0.1438, 1.02
Min. and Max. Resd. Dens.[e/Å^3]	-0.43, 0.45

Preparation of $[NiL^2]ClO_4$ (2)

Complex **2** was prepared by the same procedure as described above, except that 2,6-diformyl-4-methylphenol was used instead of 2,6-diformyl-4-fluorophenol. Yield: 0.139 g (51 %). Anal. Calc. for $C_{20}H_{23}N_4NiO_4ClO_4$ (%): C, 44.4; H, 4.3; N, 10.3 Found: C, 44.4; H, 4.3; N, 10.4. IR(KBr, ν/cm^{-1}): 3,210 ν(N–H), 1,628 ν(C=N), 1,681 ν(C=O), 1,093, 624 $\nu(ClO_4^-)$.

Crystal structure determination

The crystallographic data were measured on a Bruker AXS SMART diffractometer (Mo Kα radiation, 0.71073 Å). Data reduction and cell refinement were performed with the SMART and SAINT programs. The structures were solved by direct methods (Bruker SHELXTL) and refined on F^2 by full-matrix least squares (Bruker SHELXTL) using all unique data [9]. Hydrogen atoms were located geometrically and refined in riding mode. The non-H atoms were refined with anisotropic displacement parameters. Calculations were performed using the SHELX-97 crystallographic software package. The crystallographic data of complex **1** are summarized in Table 1, and the detailed crystallographic data of complex **2** have been reported in our previous work [12].

DNA binding experiments

The CT-DNA was dissolved in 100 mL Tris–HCl buffer (50 mM Tris–HCl, 50 mM NaCl and pH = 7.2). The concentration of CT-DNA was calculated according to Beer–Lambert's Law $A = \varepsilon bc$, where ε is the molar extinction coefficient, 6,600 $M^{-1}cm^{-1}$ $(nudeotide)^{-1}$ at 260 nm [13]. The absorption ratio A_{260}/A_{280} was within the range of 1.8–2.0, indicating that this solution was sufficiently free from protein [14]. The calculated DNA concentration was 3.47×10^{-4} M.

The UV–vis experiments were carried out at fixed concentration of the complexes (50 μM) and varying the concentration of DNA (0–50 μM). Absorption spectra were recorded using cuvettes of 1 cm path length. Before measurements, the mixtures of DNA and complex were incubated for 30 min at room temperature. The intrinsic binding constant was determined using the equation [15]:

$$[DNA]/E_{ap} = [DNA]/E + 1/(K_bE)$$

where $E_{ap} = \varepsilon_a$ _ ε_f, $E = \varepsilon_b - \varepsilon_f$, ε_a, ε_f and ε_b correspond to A_{obsd}/[Ni], the extinction coefficient for the free complex, and the extinction coefficient for the complex in the fully bound form, respectively. Plots of $[DNA]/(\varepsilon_a - \varepsilon_f)$ versus [DNA] gave the binding constant K_b as the ratio of the slope to the intercept [16].

To further clarify the interactions between these complexes and DNA, the decrease in fluorescence intensity of the EB–DNA system (EB = ethidium bromide) caused by intercalation of the complexes has been measured, as shown in Fig. 7. The experiments were performed at a fixed EB-DNA solution concentration (2×10^{-5} M EB, 2.87×10^{-5} M DNA), to which increments of the complex solutions ranging from 0 to 1.2×10^{-4} M were added. The solutions were equilibrated for 10 min before the fluorescence was recorded [17]. The Stern–Volmer quenching constant was determined from the equation $I_0/I = 1 + K[Q]$ [18], where I_0 and I are the emission intensities in the absence and the presence of the complex, respectively.

Viscosity measurements were carried out using a capillary viscometer at a constant temperature (25.0 ± 0.1 °C). Each set of data was measured three times, and the averages are presented as $(\eta/\eta_0)^{1/3}$ versus molar ratio of complex to DNA [19], where η and η_0 are the viscosity of DNA in presence and absence of the complex, respectively. Viscosity values were calculated from the observed flow times of DNA containing solutions corrected for the flow time in buffer alone (t_0), $\eta = (t - t_0)$ [20]. Flow times were measured with a digital stopwatch.

Results and discussion

Synthesis and characterization

In the IR spectra of the complexes, strong absorption bands at 1,635 cm^{-1} for **1** and 1,628 cm^{-1} for **2** are observed, which are assigned to the ν(C=N) stretching vibrations. Bands at 1,681 cm^{-1} for **1** and 1,688 cm^{-1} for **2** are attributed to the ν(C=O) stretching vibrations, indicating that there is a CHO group in each complex. The slight wavelength differences are attributed to the different substituents (–F in **1**, $–CH_3$ in **2**). Comparing the IR spectra of the free ligands and their complexes, the ν(N–H) absorption bands shift from 3,439 cm^{-1} for the free ligands to 3,209 ± 1 cm^{-1} for the complexes, consistent with coordination of the nitrogen atoms to the metal. Strong bands at 1,093 ± 1 and 624 cm^{-1} for the complexes can be attributed to the ClO_4^- anions [1]. Hence, one spectroscopic data are in agreement with the crystal structures of the complexes.

The UV–Vis spectra (see supporting material S1) of complexes **1** and **2** both show sharp absorptions at 238 nm, assigned to $\pi \rightarrow \pi^*$ inter ligand transitions, plus moderate absorptions at 432 nm for **1** and 429 nm for **2**, which may be due to the d^8 configuration of Ni^{2+}, giving rise to a charge transfer (CT) transition [21].

The ES–MS spectra of the complexes in methanol solution are shown in supporting material S2. The spectra are dominated by peaks at m/z 445.08 for **1** and 441.08 for **2**, corresponding to $[NiL^1]^+$ (calc. 445.07) and $[NiL^2]^+$ (calc. 441.10), respectively, indicating that the two cations are stable in methanol solution. These assignments are supported by the good agreement between the theoretical and experimental isotope distributions, shown in the inset of the figures.

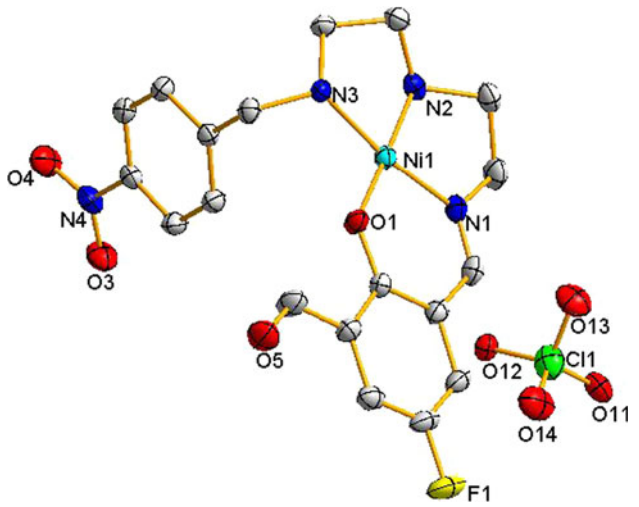

Fig. 1 Perspective views of the complex **1**. Hydrogen atoms are omitted for clarity (ellipsoids are drawn at 30 % probability level)

Crystal structures of the complexes

Perspective views of the complexes are given in Figs. 1 and 3, together with the atom numbering schemes. Selected bond lengths and angles are listed in Table 2.

The molecular structure of complex **1** contains a $[NiL^1]^+$ cation and a ClO_4^- anion. The deprotonated ligand coordinates with nickel(II) in a tetradentate manner, by means of three amine nitrogen atoms and one oxygen from phenol. This arrangement results in one six-membered chelate ring and two adjacent five-membered chelate rings. According to the literature, the angles around the nickel atom associated with five-membered chelate rings are invariably smaller than those associated with six-membered rings [22, 23]; the corresponding values in complex **1** are ∠N1–Ni1–N2 = 86.08(17)°, ∠N2–Ni1–N3 = 87.09(16)°, ∠O1–Ni1–N1 = 95.78(15)°, which are in accordance with the general trend. The coordination polyhedron of the metal center can be approximately described as square planar, such that the four coordination atoms are coplanar with a mean plane deviation of 0.032 Å, while the deviation of Ni(II) from the base plane is 0.051 Å. The two aromatic rings in the ligand are almost perpendicular, with a dihedral angle of 83.5°. The coordination bond distances are in the range of 1.825–1.944 Å, and the Ni–O distances are shorter than the Ni–N distances. In the crystal, cations and anions are linked by weak C(N)–H···O hydrogen bonding, and the relevant H-bond parameters are given in Table 3. The hydrogen bonding interactions of one molecular unit with adjacent ones are depicted in Fig. 2.

Complex **2** is almost isostructural with complex **1**, except for the different substituent on the phenyl groups, F in L^1 and CH_3 in L^2. The angles within the chelate rings around the nickel atom are ∠N2–Ni1–N3 = 86.28(13)°, ∠N3–Ni1–N4 = 85.82(14)°, ∠O1–Ni1–N2 = 96.39(14)°, respectively, similar to those of complex **1**. The hydrogen bonding interactions of one molecular unit with adjacent ones are depicted in supporting material S3.

Cyclic voltammetry

The cyclic voltammograms of the complexes were recorded in DMF solution using tetrabutyl ammonium

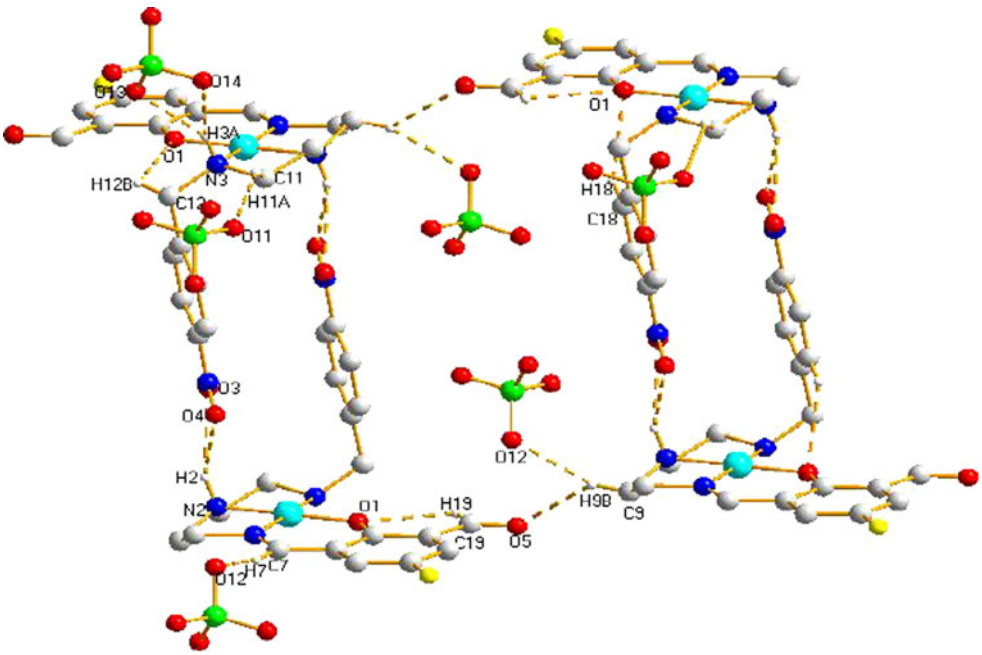

Fig. 2 View of the hydrogen bonding interactions of one molecular unit with adjacent ones in complex **1**. Hydrogen atoms except those involved in hydrogen bonding are omitted for clarity

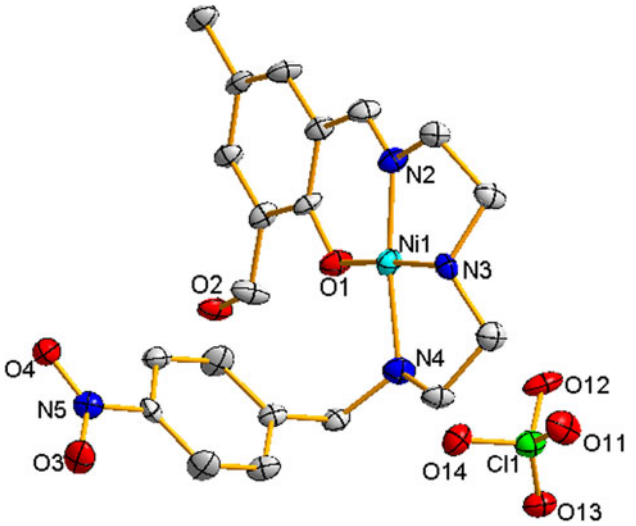

Fig. 3 Perspective views of the complex **2**. Hydrogen atoms are omitted for clarity (ellipsoids are drawn at 30 % probability level)

Table 2 Selected bond lengths (Å) and bond angles (°) for the complex **1**

Bond	Distance	Bond	Distance
Ni1–O1	1.825(3)	Ni1–N1	1.853(4)
Ni1–N2	1.895(4)	Ni1–N3	1.944(3)
Bond	Angles	Bond	Angles
O1–Ni1–N1	95.78(15)	N1–Ni1–N2	86.08(17)
O1–Ni1–N2	177.65(15)	N1–Ni1–N3	171.46(17)
O1–Ni1–N3	90.93(14)	N2–Ni1–N3	87.09(16)

perchlorate (TBAP) as supporting electrolyte in the scan range from −1.0 to −0.5 V. The scan rate was varied in the range of 50–200 mVs^{-1}, with the results shown in Fig. 4.

The cyclic voltammograms of complex **1**, showed a pair of anodic and cathodic peaks, which can be attributed to the Ni(II)–Ni(I) redox couple. For the scan at 100 mV s^{-1}, the cathodic peak potential (Epc) is −0.887 V and the anodic peak potential (Epa) is −0.746 V; the half-wave potential calculated from (Epc + Epa)/2 is −0.817 V; the separation (ΔEp) of the anodic and cathodic peak potentials is 0.141 V and the ratio of cathodic and anodic peak currents i_{pc}/i_{pa} is 2.3, indicative of a pseudo-reversible electrochemical process [9]. The values of $i_{pc}/v^{1/2}$ ($v = 50$, 100, 200 mVs^{-1}, respectively) are approximately the same, indicating that this process is mainly diffusion controlled [1]. In complex 2, at a scan of 100 mV s^{-1}, E1/2 = −0.816 V, ΔEp = 0.134 V, $i_{pc}/i_{pa} = 2.3$, again characteristic of a pseudo-reversible electrochemical process.

Table 3 Hydrogen bonding distances (Å) and angles (°) for the complex **1**

D–H···A	d (D—H) Å	d(H···A) Å	D(D···A) Å	∠DHA°
N2–H2···O3	0.9100	2.5500	3.369(5)	150.00
N2–H2···O4	0.9100	2.3700	3.136(6)	142.00
N3–H3A···O13	0.9100	2.2100	3.015(6)	147.00
N3–H3A···O14	0.9100	2.5200	3.332(7)	149.00
C7–H7···O12	0.9300	2.4300	3.324(5)	161.00
C9–H9B···O5	0.9700	2.5200	3.259(6)	133.00
C9–H9B···O12	0.9700	2.4400	3.292(6)	146.00
C11–H11A···O11	0.9700	2.4700	3.185(5)	130.00
C12–H12B···O1	0.9700	2.5900	3.017(5)	107.00
C15–H15···O5	0.9300	2.5600	3.271(6)	133.00
C18–H18A···O1	0.9300	2.5900	3.324(5)	136.00
C19–H19···O1	0.9300	2.4400	2.768(6)	101.00

UV spectroscopic studies

Electronic absorption spectroscopy is a useful technique for characterization of the binding mode between metal complexes and DNA [24]. The UV absorption spectra of the complexes are shown in Figs. 5 and 6. Complex **1** shows a moderate absorption at 431 nm, which can be assigned to a charge transfer transition. Upon the addition of CT-DNA solution, the spectrum of complex **1** shows obvious hyperchromicity, up to about 17 %. The hyperchromic effect might be ascribed to electrostatic binding, or to partial uncoiling of the helix structure of DNA, making the DNA bases more exposed [3, 25]. The value of binding constant K_b obtained from the plot of [DNA]/E_{ap} versus [DNA] is 5.43×10^5 M^{-1}.

The UV absorption spectrum of the complex **2** also shows absorption at 431 nm, but addition of DNA now results in hypochromism, reaching a maximum of about 14 %. The binding constant $K_b = 1.83 \times 10^5$ M^{-1}, indicating that complex **2** interacts with DNA by intercalation, involving strong stacking interactions of the aromatic chromophore of the complex with the DNA base pairs. Comparing the DNA binding constants of the complexes with those of similar mononuclear Ni(II) complexes [26–29], it is found that all these complexes have considerable binding capacity. Although the DNA binding constants vary with their structural differences, the interaction modes of these complexes with DNA are all intercalative. There is no obvious relationship between the structures of the complexes and their DNA binding properties. Nevertheless, considering that the interaction mode of DNA with these complexes is intercalative, the aromatic groups in the complexes are likely to play an important role in the binding.

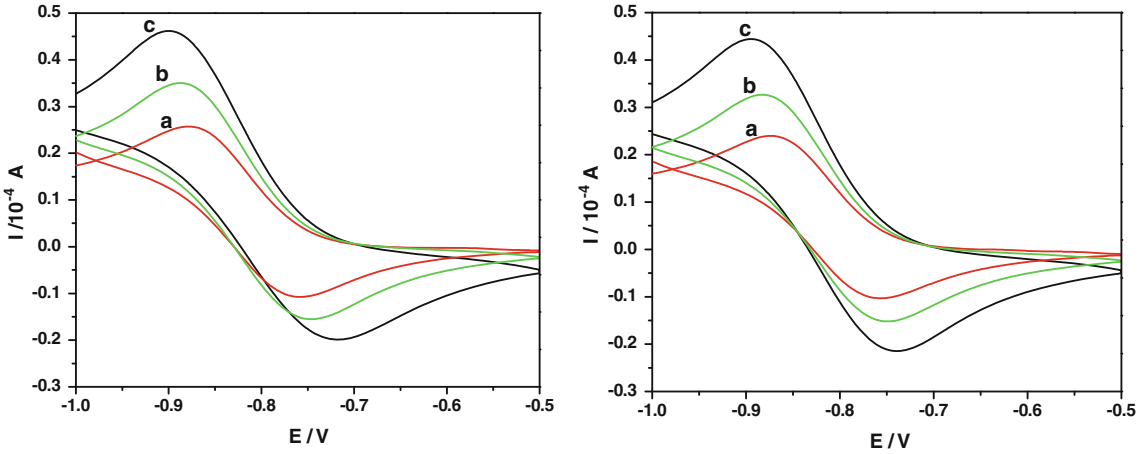

Fig. 4 Cyclic voltammograms in DMF solution in the range from −1.0 to −0.5 V (supporting electrolyte = TBAP, 0.1 M), Scan rate, $\nu_a = 50$ mV s^{-1}, $\nu_b = 100$ mV s^{-1}, $\nu_c = 200$ mV s^{-1} (left: complex **1**, right: complex **2**)

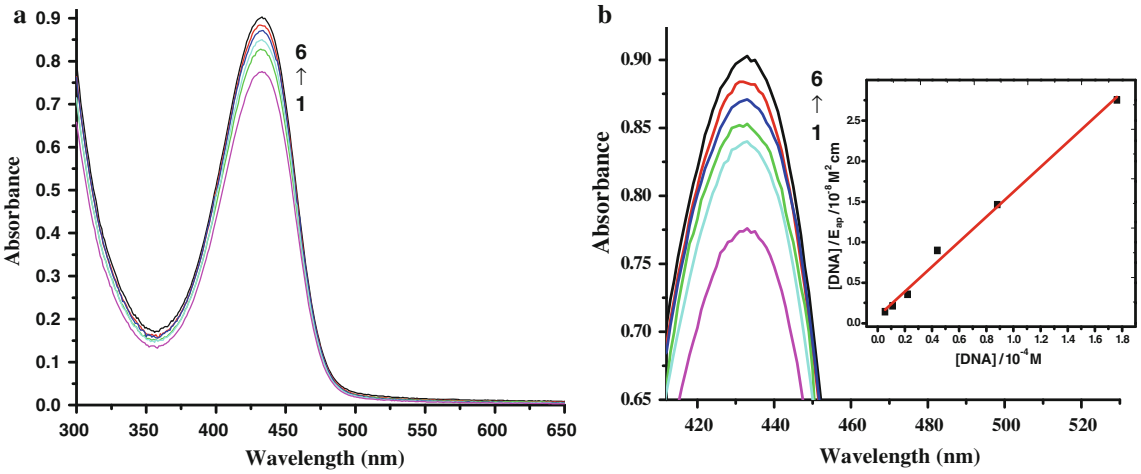

Fig. 5 **a** Absorption spectra of complex **1** in Tris–HCl buffer (pH = 7.2) solution upon addition of DNA. [complex **1**] = 100 μM, [DNA] = 0 – 0.87 μM. *Arrows* show the absorption changes upon increasing the concentration of DNA. **b** *Enlarged plot* of the absorption changes at 431 nm and plot of [DNA]/E_{ap} versus [DNA] for complex **1**

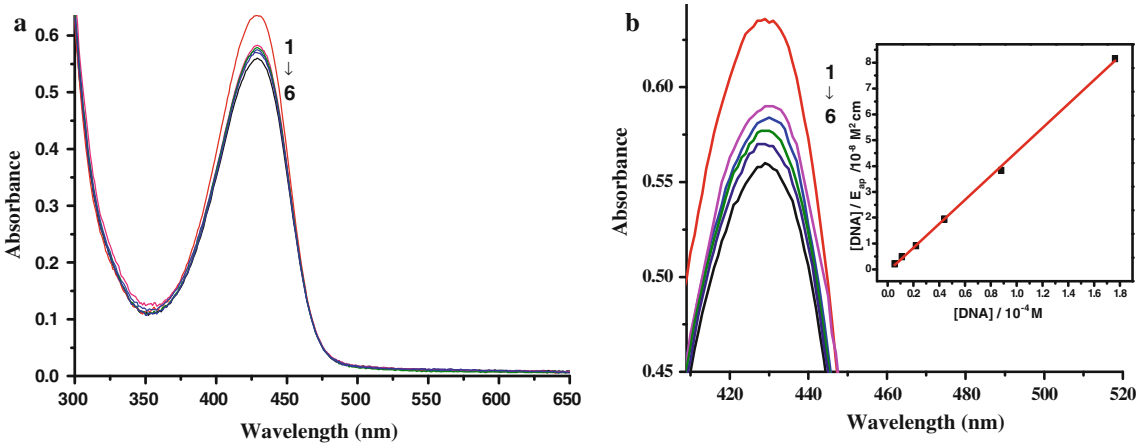

Fig. 6 **a** Absorption spectra of complex **2** in Tris–HCl buffer (pH = 7.2) solution upon addition of DNA. [complex **2**] = 100 μM, [DNA] = 0–0.87 μM. *Arrows* show the absorption changes upon the increasing concentration of DNA. **b** *Enlarged plot* of the absorption changes at 431 nm and plot of [DNA]/E_{ap} versus [DNA] for complex **2**

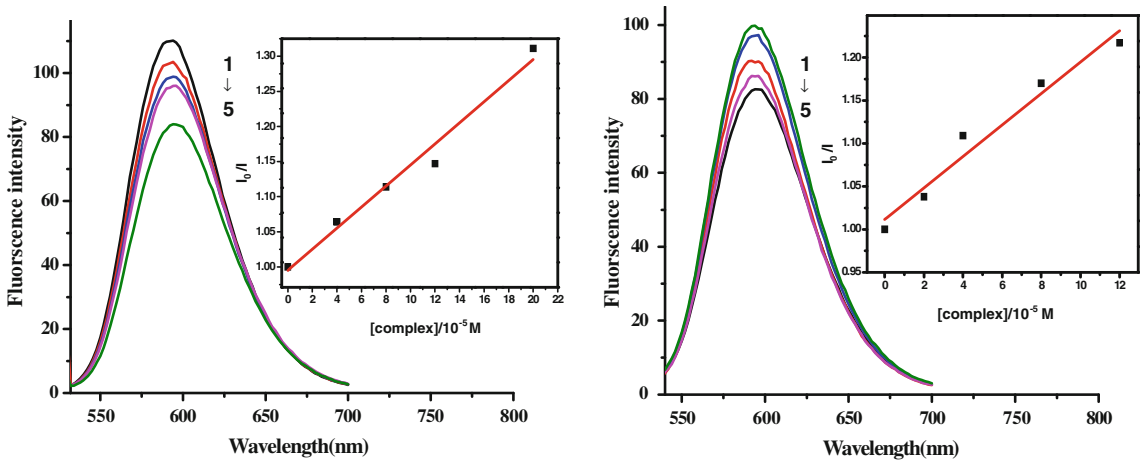

Fig. 7 Emission spectra of EB bound to DNA in the absence (*1*) and presence (*2–5*) of the complexes. Inset Stern–Volmer quenching plots of EB bound to DNA. [EB] = 20 μM, [DNA] = 28.7 μM, [complex] 1–5 = 0–200 μM; λex = 520 nm (*left*: complex **1**; *right*: complex **2**)

Fluorescence spectroscopic studies

In order to further investigate the binding of these complexes to DNA, their ability to displace EB from the intercalated EB-DNA complex was investigated [2, 25]. Emission spectra of the EB-DNA system in the absence and presence of the complexes and the associated Stern–Volmer quenching plots are shown in Fig. 7. The emission spectra of EB bound to DNA exhibit a single peak at 596 nm. As the concentration of complex **1** is increased, the emission intensity decreases. The linear Stern–Volmer quenching constant obtained from the slope of the plot of I_0/I versus [Q] is 0.83×10^3 $M^{-1}$for complex **1**.

The same situation occurs for complex **2**; the emission intensity decreases as the concentration of complex **2** is increased, and the linear Stern–Volmer quenching constant K_{SV} is 0.71×10^3 M^{-1}, which is very similar to that of a dinuclear nickel(II) complex with a similar ligand containing three phenzyl groups [9]. However, the binding constant of **2** is 4.3 times lower than that of the dinuclear nickel(II) complex, suggesting a synergetic effect of the metal centers in DNA binding. The binding and quenching constants of complex **1** are larger than those of **2**, which can be only ascribed to the different substituents. The fluorine atom in **1** can interact with the adjacent phenyl group; together with its smaller steric requirement, this would increase the π–π stacking interaction between the base pairs of DNA and complex **1**, leading to a stronger interaction.

Viscosity studies

Viscosity measurements are usually regarded as an effective physical method for the characterization of DNA binding mode, since intercalation into the DNA base pairs will loosen the DNA helix structure, resulting in the overall increase of DNA length and so increasing the DNA solution viscosity. In contrast, hydrogen bonding and van der Waals interactions along the groove produce no significant change in the viscosity of DNA solutions [30].

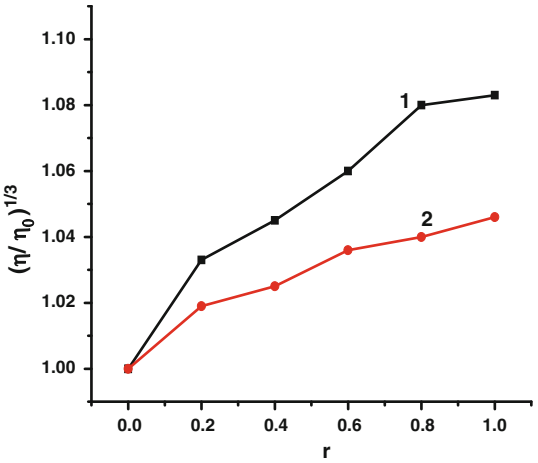

Fig. 8 Effects of increasing amounts of complexes **1** and **2** on the relative viscosities of CT-DNA solutions at 25.0 ± 0.1 °C; [DNA] = 200 μM, *r* = [complex]/[DNA]

The results of viscosity studies are shown in Fig. 8. As the concentration of the complexes is increased, the viscosity of the DNA solution also increases, providing further evidence that the binding mode of the complexes with DNA is intercalation. The effect of complex **1** on the viscosity is much higher than that of **2** at the same ratio of DNA/[complex], revealing that the complex **1** intercalates more strongly than **2**. This result is in agreement with the observation that the binding constant of **1** is 3 times larger than that of **2**.

Conclusions

Two unsymmetrical mononuclear nickel(II) complexes with different substituents have been prepared and characterized by spectroscopy, cyclic voltammetry and single crystal X-ray diffraction. The DNA binding abilities vary somewhat with the substituent, such that binding of the F-substituted complex is higher than that of CH_3-substituted complex. Comparison of these results with those available in the literature suggests that a synergetic effect from more than one metal center would increase the DNA binding ability.

Supplementary material

Crystallographic data have been deposited with the Cambridge Crystallographic Data Center. The CCDC number of complex **1** is 950658. Copy of the data can be obtained free of charge on application to The Director, CCDC, 12 Union Road, Cambridge CB2, 1EZ, UK (fax: +44-1223-336033); E-mail: deposit@ccdc.cam.ac.uk or http://www.ccdc.cam.ac.uk).

Acknowledgments We acknowledge financial support from the Natural Science Foundation of China (21171135 and 20971102) and China Hubei Provincial Science & Technology Department (2011BFA020).

References

1. Cheng QR, Chen JZ, Zhou H, Pan ZQ (2011) J Coord Chem 64:1139–1152
2. Wang HY, Yuan WB, Zhang Q, Chen SW, Wu SS (2008) Trans Met Chem 33:593–596
3. Wu HL, Jia F, Kou F, Liu B, Yuan JK, Bai Y (2011) Trans Met Chem 36:847–853
4. Golbedaghi R, Salehzadeh S, Keypour H, Blackman AG (2010) Polyhedron 29:850–856
5. Kumar RS, Arunachalam S (2007) Polyhedron 26:3255–3262
6. Bauer-Siebenlist B, Meyer F, Farkas E, Vidovic D, Cuesta-Seijo JA, Herbst-Irmer R, Pritzkow H (2004) Inorg Chem 43: 4189–4202
7. Krishna ER, Reddy PM, Sarangapani M, Hanmanthu G, Geeta B, Rani KS, Ravinder V (2012) Spectrochim acta Part A: molecular and biomolecular. Spectroscopy 97:189–196
8. Kimura E, Kodama Y, Koike T, Shiro M (1995) J Am Chem Soc 117:8304–8311
9. Wang Y, Xiao W, Mao JW, Zhou H, Pan ZQ (2013) J Mol Struct 1036:361–371
10. Long RC, Hendrickson DN (1983) J Am Chem Soc 105: 1513–1521
11. Mandal SK, Thompson LK, Newlands MJ, Gabe EJ (1989) Inorg Chem 28:3707–3713
12. Wang Y, Mao JW, Song HT, Zhou H (2012) Acta Cryst E 68:766
13. Reichmann ME, Rice SA, Thomas CA, Doty P (1954) J Am Chem Soc 76:3047–3053
14. Marmur J (1961) J Mol Biol 3:208–218
15. Uma V, Kanthimathi M, Subramanian J (2006) J Biochim Biophys Acta 1760:814–819
16. Wolfe A, Shimer GH, Meehan T (1987) Biochemistry 26: 6392–6396
17. Wang XL, Fang JN, BI YF, Lin HY, Liu GC (2008) Chem Res Chinese U 24:15–19
18. Ivanov VI, Minchenkova LE, Schyolkina AK, Poletayer AI (1973) Biopolymers 12:89–110
19. Liu ZC, Yang ZY, Li TR, Wang BD, Li Y, Wang MF (2011) Trans Met Chem 36:489–498
20. Tan CP, Liu J, Chen LM, Shi S, Ji LN (2008) J Inorg Biochem 102:1644–1653
21. Sun L, Li YG, Dong XW, Guo MX (2012) Trans Met Chem 37:361–366
22. Schlemper EO, Murmann RK, Hussain MS (1986) Acta Crystallogr Sect C 42:1739–1743
23. Hussain MS, Schlemper EO (1979) J Inorg Chem 18:2275–2285
24. Kelly TM, Tossi AB, McConnell DJ, Strekas TC (1985) Nucl Acids Res 13:6017–6034
25. Psomas G (2008) J Inorg Biochem 102:1798–1811
26. Xu J, Chen YF, Zhou H, Pan ZQ (2011) J Coord Chem 64: 1626–1635
27. Wang QX, Li WQ, Liu AF, Zhang B, Gao F, Li SX, Liao XL (2011) J Mol Struct 985:129–133
28. Selvarani V, Annaraj B, Neelakantan MA, Sundaramoorthy S, Velmurugan D (2013) Polyhedron 54:74–83
29. Ramadan AEMM (2012) J Mol Struct 1015:56–66
30. Sadhukhan D, Ray A, Das S, Rizzoli C, Rosair GM, Mitra S (2010) J Mol Struct 975:265–273